5706

Calculation of buoyant air movement in buildings – proposals for a numerical benchmark test case

J J McGUIRK, PhD, DIC, ACGI
Loughborough University, UK
G E WHITTLE, MSc, PhD, CEng, MIMechE
Arup Research and Development, London, UK.

SYNOPSIS A numerical benchmark test problem is proposed to highlight particular modelling issues which arise in buildings. Alternative solution stragegies are discussed in the context of the challenges which building air flow analysis offers to both CFD code developers and practitioners.

NOTATION

D	slot width
F	Froude number
t	time
V_x	velocity at distance x
V_o	jet discharge velocity
V_1	dimensionless velocity
x	distance
x_1	dimensionless distance

1 INTRODUCTION

Methods based on computational fluid dynamics (CFD) are beginning to make a significant impact in the evaluation of air distribution particularly for large, unconventional or critical spaces. The methods are proving to be very powerful but it is clear they must be used with care to get the best from them - despite the everyday nature and apparent simplicity of building flows the accurate calculation of air distribution poses a considerable challenge to both code developers and practitioners. In other fields where CFD is contributing to design methods (eg. aerospace), benchmark test problems and validation studies are playing an important development role. The test problems should of course highlight the physical and numerical modelling issues most relevant to the particular application. In the context of building services / air movement, these include:

(i) resolution of features with a range of geometric scale, from supply air diffusers (of order of millimetres) to room dimensions (of order of 10 metres);

(ii) high amplitude and low frequency velocity fluctuations, which are characteristic of transition and low Reynolds number flow;

(iii) a mix of forced and free convection at surfaces (over a wide range of Rayleigh number);

(iv) prediction of wall convective heat transfer rates;

(v) accurate and robust convective discretisation.

These aspects will impact upon the choice of optimum physical and numerical modelling approaches, including:

(a) mesh type and method of construction;

(b) relative efficiency / desirability of iterative or time-resolved algorithms;

(c) degree of sophistication of turbulence model / high or low Reynolds number effects / buoyancy extension / near-wall treatment;

(d) efficiency / ease of approach to mesh independent solutions.

There are clearly many issues to consider in the application of CFD in this field, and there is a need for one or more representative numerical benchmark problems which embody the characteristics and features which predominate in buildings. This paper proposes one possible benchmark problem and describes alternative solution strategies in the context of the challenges offered.

2 BACKGROUND

One of the first to use CFD for prediction of air movement in buildings was Nielsen [1], who, in 1974 used a two-dimensional stream function-vorticity code for computing isothermal flows. The code was based on earlier (1969) work by Gosman et al [2] on the prediction of recirculating flows. Later developments led to the ability to simulate three-dimensional flows by solving for velocity components and pressure (primitive variables) using a pressure-correction method within the finite-volume framework [3]. The influence of buoyancy was introduced by calculation of temperature from the energy conservation equation and then buoyancy force (for use in the momentum equations) either using the Bousinesq approximation or from density gradient via the 'ideal gas' law.

The use and progress of CFD in buildings in the period up to 1986 is outlined and reviewed in [4]. More recent developments, based on a review of air movement modelling in buildings, is described in [5].

Regarding numerical benchmark cases for building services / room air movement applications, relevant work is being undertaken on the collaborative International Energy Agency Annex 20 project entitled 'Air flow patterns in buildings'. Here, measurements are being performed in a number of test rooms and simulations are being carried out using different codes. Work is being done in Europe and North America. The test rooms are sized 4.2m x 3.6m x 2.5m height and experiments are being performed representing isothermal forced convection, summer cooling (mixed convection) and winter heating with a radiator beneath a window (free convection). Comparisons are made between measurement and prediction based on profiles of velocity, temperature and turbulence quantities, and on mean comfort-related parameters. Some work is also being carried out in measuring and predicting the transport of light, neutral and heavy contaminants. The diffuser used in the tests comprises a large number of tiny nozzles and is, not surprisingly, proving difficult to model.

Additionally, as part of the work programme a near two-dimensional case has been selected which uses a simple slot opening through which ventilation air is introduced. This case, which is somewhat easier to model, is based on measurements and predictions described by Nielsen et al [6]. Isothermal and buoyant cooling flow are being considered. For the former, profiles of velocity and turbulence quantities are being compared, and for the latter the critical Archimedes number (the ratio of buoyancy to inertia) at which flow reversal occurs is being identified. Both two-dimensional and three-dimensional simulations of this test case have been performed. Substantial amounts of data have already come forward from this project [7], which should provide the basis for defining future benchmark cases. However, the three-dimensionality of most of the flows means that mesh-independent calculations are currently difficult, if not impractical, to achieve.

Benchmark test cases have been proposed by Baker and Kelso [8,9] associated with work being undertaken for ASHRAE. The proposed cases are based mainly on simplified isothermal flows and also on existing room air measurements by Lorch and Straub [10] and Nelson and Stewart [11]. The particular ASHRAE project is focused on the development and testing of a finite-element CFD code for room air movement applications. Here, the simplified cases such as isothermal flow over a backward-facing step and the lid-driven cavity are of limited interest to those investigating optimum CFD performance in room air movement applications; whilst the three-dimensional benchmark cases suffer from the same limitations outlined above.

It is these considerations regarding the appropriateness of existing benchmark test cases which have led to the proposals discussed in this paper.

3 SELECTION OF TEST CASE

In the work described here attention is focused on two-dimensional isothermal and buoyant vertical jets. In a building services context this comprises a cold jet projected vertically downwards from the ceiling. Interest is in the velocity decay of the jet and, in the case of buoyant flow, the transition of the jet behaviour from an initially non-buoyant regime through an intermediate stage to the condition where the jet behaves as a pure plume. Chen and Rodi [12] have discussed the behaviour of vertical buoyant jets in some detail.

The plane (two-dimensional) jet is selected because it can be calculated in great detail much more readily and with more modest computing resources than had a three-dimensional case been selected.

The particular test case comprises a room module cross-section 5m x 5m height, with a 2cm wide shot in the ceiling. Figure 1 shows a schematic of the space with the supply air slot and exhaust locations in the ceiling. Calculations have been made for supply velocities of 1.0 and 1.5m/s and for a supply temperature of 20°C. The heat gain in the space is introduced by imposing a surface temperature of 24°C (for the floor and ceiling) and convective heat transfer coefficient of $3W/m^2°C$, and/or by prescribing a volumetric heat flux rate. Both methods

are representative of how thermal boundary conditions are set in CFD simulations of the indoor environment.

4 SIMULATIONS

Two codes have been used in the analysis. Both are finite-volume, both solve on a staggered grid and both offer steady-state or time-dependant operation.

One code [13], which uses a pressure-correction approach solves on an arbitrary single-block, non-orthogonal, curvilinear mesh. Although, in the simulations performed here, only a cartesian mesh was used. The code incorporates a standard high Reynolds number buoyancy-extended k-ε turbulence model and also a full second-moment closure model for Reynolds stresses and heat fluxes. For the present study only the eddy viscosity (k-ε) model was used. Alternative differencing schemes comprising HYBRID and QUICK are selectable. The HYBRID scheme uses upwind differencing (with diffusion suppressed) at high Peclet number and central differencing at low Peclet number. The QUICK scheme is second order accurate but can under certain circumstances exhibit under- or over-shoots in solution variable, and delayed convergence.

In the second code, a pressure-coupled formulation on a cartesian grid is used. This latter code (AIRFLO) has been developed within Arup Research and Development specifically for buildings applications. Here, velocity components and pressure are solved concurrently within each iteration/time-step rather than in a segregated way. The equation for pressure is obtained by substituting momentum equations for the velocity components which would otherwise appear in the mass continuity equation [14]. Re-arranging then results in a diagonally dominant equation for pressure. The equation is exact thus obviating the need for a pressure-correction procedure. A Gauss-Seidel point-by-point solver with multi-directional sweep through the domain is used. In these simulations the enhanced diffusional effects of turbulence are accounted for by prescribing an eddy-viscosity which is two orders of magnitude higher than the laminar value. The basis for this follows from a consideration of length-scale and turbulence intensity in the supply from the diffuser and in the room. The energy equation is solved (for temperature) in the usual segregated way.

Simulations have been performed for the isothermal and buoyant jets at supply velocities of 1.0 or 1.5m/s and with a range of heat gains, as indicated below:

(i) isothermal jet;

(ii) buoyant jet, with surface temperature of 24°C, giving a temperature difference of approximately 1.5 to 2.0°C;

(iii) buoyant jet with surface temperature of 24°C and volumetric heat flux in the lower 1.5 to 1.8m height, giving a temperature difference in the range 2.5°C to 5.0°C;

(iv) buoyant jet with a volumetric heat flux in the whole space, giving a temperature difference of approximately 10°C. For a supply temperature of 20°C, this results in a mean room temperature much higher than would normally be acceptable for thermal comfort. However, the higher gain was introduced to ensure that for this case the jet became fully buoyant and could be compared more readily with experimental / empirical data. The results, with temperature re-referenced, are comparable to the situation with a supply air temperature of, say, 14°C and room of 24°C.

Calculations have been performed on both a half-mesh, recognising symmetry about the slot centre-line, and a full mesh. The full-mesh was specified in order to give the potential to capture any underlying time-dependency of the flow under strong buoyancy effects.

The mesh resolutions were 40x40 for the half-mesh, and 21x10, 41x20 and 80x40 for the full mesh. Figures 2 to 5 show the meshes used.

Mainly, steady-state calculations have been performed although for the strong buoyancy case (a temperature difference of 10°C) time-dependant calculations were necessary.

Simulations were made on SUN Sparc 1 and IPC workstations.

5 RESULTS OF SIMULATIONS

Results are presented in the form of flow patterns, transverse velocity and temperature across the jet, velocity decay with distance from the slot, and velocity and distance modified by Froude number. Froude number is the ratio of inertia to buoyancy and is the inverse of Archimedes number. It is used by Chen and Rodi [12] to compare the performance of buoyant jets.

Comparative examples are also shown of convergence histories of buoyant flow.

5.1 Isothermal flow

5.1.1 Differencing scheme

Calculations were first carried out for an isothermal situation on a 40x40 mesh (over half the room), switching the convection discretisation scheme from first order HYBRID differencing to second order QUICK differencing. The results, Figure 6, for centre-line velocity, show little change. This implies that numerical diffusion effects are negligibly small even with first order differencing for this problem with this mesh density. This is due to the fact that over most of the flow domain the flow is aligned with the mesh lines (see velocity vectors, Figure 7). Further, the high levels of effective viscosity generated (see Figure 8) means that in all probability, even in the HYBRID predictions, the cell Peclet numbers for the transverse (horizontal) direction coefficients (the direction in which the dominant diffusion occurs) will be sufficiently small for the coefficients to be second order central differenced. This particular flow is therefore not very sensitive to discretisation errors, as long as mesh densities of this order are used (this of course might not be possible in a three-dimensional version of this flow). A scenario which would be a more stringent test of the numerical accuracy of a CFD code would be where a cold jet was discharged at some oblique angle to the mesh lines (perhaps associated with flow along a sloping part of the ceiling), and fell away across the mesh due to buoyancy. This would form an interesting and numerically more demanding variant of the test problem considered here.

5.1.2 Mesh resolution

Isothermal calculations were also made on three full-meshes, of resolution 21x10, 41x20 and 80x40. The flow pattern are shown in Figures 9 to 11. In each case, the jet projects down into the space with velocity reducing as momentum diffuses sideways from the jet in the horizontal directions.

Figure 12 shows in dimensionless form the decay of the centre-line velocity in comparison to idealised empirical data [12]. The coarse mesh result is quite different to the medium and fine mesh calculations. The graph suggests that the finest mesh calculation will not change substantially with further refinement. This was confirmed by the tests with higher order differencing on the equivalent 40x40 half-mesh described above. The comparison with the idealised relationship is encouraging and suggests that the simplified assumption of a constant eddy viscosity does not result in serious inadequacies. The value used of 100 x laminar was consistent with that predicted above by the k-ε model, at least for the jet region, although much higher values were predicted in the centre of the recirculation areas. In practice, the transition from a dimensionless velocity of unity will be smoother than that shown in the idealised curve.

5.2 Influence of buoyancy

Various runs were made on the half-mesh to examine buoyancy effects. Initially the jet velocity was fixed at 1.5m/s and wall heat transfer introduced on the floor and ceiling (wall temp 24°C, jet temp 20°C, wall heat transfer coefficient 3W/m^2°C). This produced only marginal buoyancy effects (see the centre-line velocity decay in Figure 13), with the cold jet maintaining its momentum slightly longer than in the isothermal case. The jet centre-line temperature behaviour shows (Figure 14) that the jet temperature rises only to about 21.5°C, so that differences between jet and room air densities are too small to cause significant effects. Inclusion or exclusion of buoyancy source terms in the turbulence model equations produced, not surprisingly, no differences.

Increased buoyancy was introduced by firstly lowering the jet velocity to 1.0m/s whilst retaining the wall heat transfer conditions, and at the same time, introducing a distributed heat release in the lower 1.8m of the room, initially equal to 8W/m^3. Figure 15 shows the effect on centre-line velocity and temperature development.

Temperatures of order 22.5°C are now observed in the jet and the process of reducing the rate of velocity decay (due to the accelerating effect of a cold jet surrounded by warm air) has been enhanced so that a plateau-like region appears in the decay curve, until impingement on the floor reduces the velocity.

Profiles of vertical velocity and temperature across various horizontal lines at different heights above the floor are given in Figures 16 to 19 for the weakly buoyant case. Figures 16 and 18 show results for the entire width of the solution domain, whilst Figures 17 and 19 concentrate on the immediate jet vicinity. Typical jet-like (Gaussian) profiles are observed with the spread of momentum and heat into the room space clearly visible. The shape of these profiles underlines the comments above on a vertical direction dominated by convection and a horizontal direction dominated by diffusion. The velocity profiles show the zero velocity at the 'eye' of the recirculating vortex formed in the room (see streamline pattern in Figure 20). The temperature profiles indicate the room bulk temperature in this case to be only around 21.7°C as mentioned above.

Buoyant calculations were also performed on the finest of the full-meshes (80x40), which was equivalent to the 40x40 half-mesh. These were made with the supply

velocity of 1.0m/s. Increasing heat gains were applied to ensure that sufficient buoyancy was introduced into the calculation. At the highest heat gain (10°C temperature difference) the calculation had to be performed time-dependant. Here, a deflection and an undulating flow in the jet was observed. A series of flow fields are shown (mainly in the form of speed contours) in Figures 21 to 28 which represent snapshots at time intervals of 10sec. It is clear that the jet velocity is being largely maintained (by the buoyancy force) within the main body of the jet and it is only impingement on the floor which causes its final decay. It is, however, interesting to note that the slow undulation of the jet causes a periodic 'breaking' of the plume at mid length.

Figure 29 shows the dimensionless velocity decay compared to data from Chen and Rodi [12]. The three regimes comprising a non-buoyant, a buoyant plume and an intermediate region are identified on the graph. The simulated data indicates that the jets do become buoyant, although the intermediate region is not particularly well defined, and undoubtedly the proximity of the floor is distorting the results at the buoyant plume end of the graph.

5.3 Convergence rate

A record was made of the iterative convergence rate of the buoyant calculations on the three meshes. In carrying out the finer mesh calculations the option used was to re-start the calculations from linearly interpolated coarser mesh results. For comparison, convergence rate is also shown for a fine-mesh calculation started from zero initial velocity fields and uniform temperature. Some coarse-mesh iterations were initially run isothermally to generate a flow field before activating the temperature calculation. For the isothermal iterations the velocity relaxation was set to 0.7 (using the pressure-coupled method, pressure is not under-relaxed). For the weakly buoyant flows the velocity relaxation was set to 0.4 and temperature relaxation to 0.8. But for buoyant flows with volumetric heat fluxes in the domain (but not at the maximum heat gain simulated) the fine grid calculation required relaxation to be tightened to 0.1 (with temperature relaxation still at 0.8).

It can be seen from Figures 30 and 31 that there is an advantage in re-starting from interpolated coarser results. For example, 1800 iterations were performed for the weakly buoyant case (no volumetric heat gains) resulting in residuals between a factor of two and an order of magnitude lower, and a reduced execution time because some of the 1800 iterations were done on the coarser meshes. The benefit accrues from the characteristic that in general, for finite-volume codes, coarse-mesh solutions are easier to obtain than fine-mesh solutions. Multigrid methods, which actively iterate between meshes of differing resolution, sometimes show dramatic improvements in convergence rate over single-grid methods. In the calculations reported here, the behaviour of the iterations is such that on re-starting, the errors dramatically increase then reduce at a relatively high rate before slowing. As stated above, overall there is some benefit with this approach including the ability to assess mesh dependency.

Figure 32 shows the convergence rate for 3000 iterations of the medium buoyancy calculation, where for the finest mesh the velocity relaxation was reduced to 0.1. Degradation of convergence rate follows from increased mesh resolution and increased under-relaxation to retain stability (in buoyant flow).

The execution time on SUN Sparc hardware (Sparc 1 and IPC) was approximately 1200 steady-state iterations per hour on the finest (80x40) mesh.

For the strong buoyancy calculations (10°C temperature difference) on the fine mesh, time-dependant calculations were performed since steady-state iterations would not converge. The time-step was set to 0.1sec and over-relaxation of pressure (relaxation= 1.5) was imposed. For these calculations, the ratio of CPU time to simulation time was approximately 60. That is, one minute of CPU time was required for each second of simulation.

6 CONCLUSIONS

A proposal is made for a numerical benchmark test case based on two-dimensional isothermal and buoyant vertical jets.

Predictions of velocity profile in the isothermal jet reproduce the expected Gaussian form, and velocity decay broadly matches empirical data.

Viscosity ratios predicted by the k-ε turbulence model show that for the jet development region the eddy-viscosity is approximately two orders of magnitude higher than the laminar value, although in the centre of the recirculation areas it is considerably higher. The assumption of a constant eddy-viscosity has resulted in realistic and representative predictions of jet performance.

For meshes of 40x40 (in the half space) QUICK differencing shows no significant advantage. However, in an equivalent three-dimensional space, meshes of 80x80x40 or greater may currently be prohibitive. Coarser three-dimensional meshes could therefore benefit from use of higher-order differencing, although, generally speaking, further work is

needed to identify and evaluate accurate and robust schemes. An extension of the test case to include a jet projected obliquely to the mesh would highlight the importance of higher order convection discretisation.

For non-isothermal jets, velocity profile and decay are influenced by buoyancy force in the expected way, and evidence exists that the transition to a buoyant plume characteristic is reproduced. Under strong buoyancy a time-dependant behaviour of the jet was observed, which would not have been evident by simulation on a half-mesh alone. An increased height of space would give opportunity for the characteristic of the jet under strong buoyancy to be more clearly identified.

Convergence histories for even relatively weakly-buoyant flow demonstrate the degradation in convergence rate associated with buoyancy.

It is proposed that the benchmark test case discussed here, or a variant of it, is more suitable for investigating optimum CFD performance in room air movement applications than other benchmarks suggested to date. Although in this work comparisons have been made with experimental data, there could be benefit to be gained in adding to our understanding of the physical mechanisms at work through further practical experimentation.

7 REFERENCES

(1) Neilsen, P.V. Flow in air conditioned rooms. PhD Thesis, Technical University of Denmark, Copenhagen, 1974.

(2) Gosman, A.D., Pun, W.K., Runchal, A.K., Spalding, D.B. and Wolfshtein, M. Heat and mass transfer in recirculating flows. Academic Press, London, 1969.

(3) Patankar, S.V. Numerical heat transfer, Hemisphere Pub., Washington DC, USA, 1980.

(4) Whittle, G.E. Computation of air movement and convective heat transfer within buildings. Int. J. Ambient Energy, Ambient Press Ltd, 1986.

(5) Jones, P.J. and Whittle, G.E. Computational fluid dynamics for building air flow prediction - current status and capabilities. Submitted for publication in Building and Environment Journal, 1991.

(6) Neilsen, P.V., Restivo, A. and Whitelaw, J.H. The velocity characteristics of ventilated rooms. Trans. ASME Journal of Fluids Engineering, vol 100, pp 291-298, 1978.

(7) Whittle, G.E. Evaluation of measured and computed test case results from IEA Annex 20. 12th AIVC Conf. Ottawa, Canada, 24-27th September 1991.

(8) Baker, A.J. and Kelso, R.M. Calculation of room air motion. ASHRAE Research project 464-RP, University of Tennessee, Knoxville, USA, June 1989.

(9) Baker, A.J. and Kelso, R.M. On validation of computational fluid dynamics: procedures for room air motion prediction. ASHRAE Trans., vol 96, pt 1, 1990.

(10) Lorch, F.A. and Straub, H.E. Performance of overhead slot diffusers with simulated heating and cooling conditions. ASHRAE Trans., Vol 89, pt 1B, 1983.

(11) Nelson, D.W. and Stewart, D.J. Air distribution from side wall outlets. ASHRAE Trans., chapter 1076, 1938.

(12) Chen, C.J. and Rodi, W. Vertical turbulent buoyant jets - a review of experimental data. Pergamon Press, Oxford, 1980.

(13) McGuirk, J.J. and Papadimitriou, C. Stably stratified free surface sheer layers with internal hydraulic jumps. In 'Stably stratified flows and dense gas dispersion', Edited by J. Pullock, Oxford University Press, 1988.

(14) Zedan, M. and Schneider, G.E. A coupled strongly implicit procedure for velocity and pressure computation in fluid flow problems. Numerical Heat Transfer, vol 8, pp 537-557, 1985.

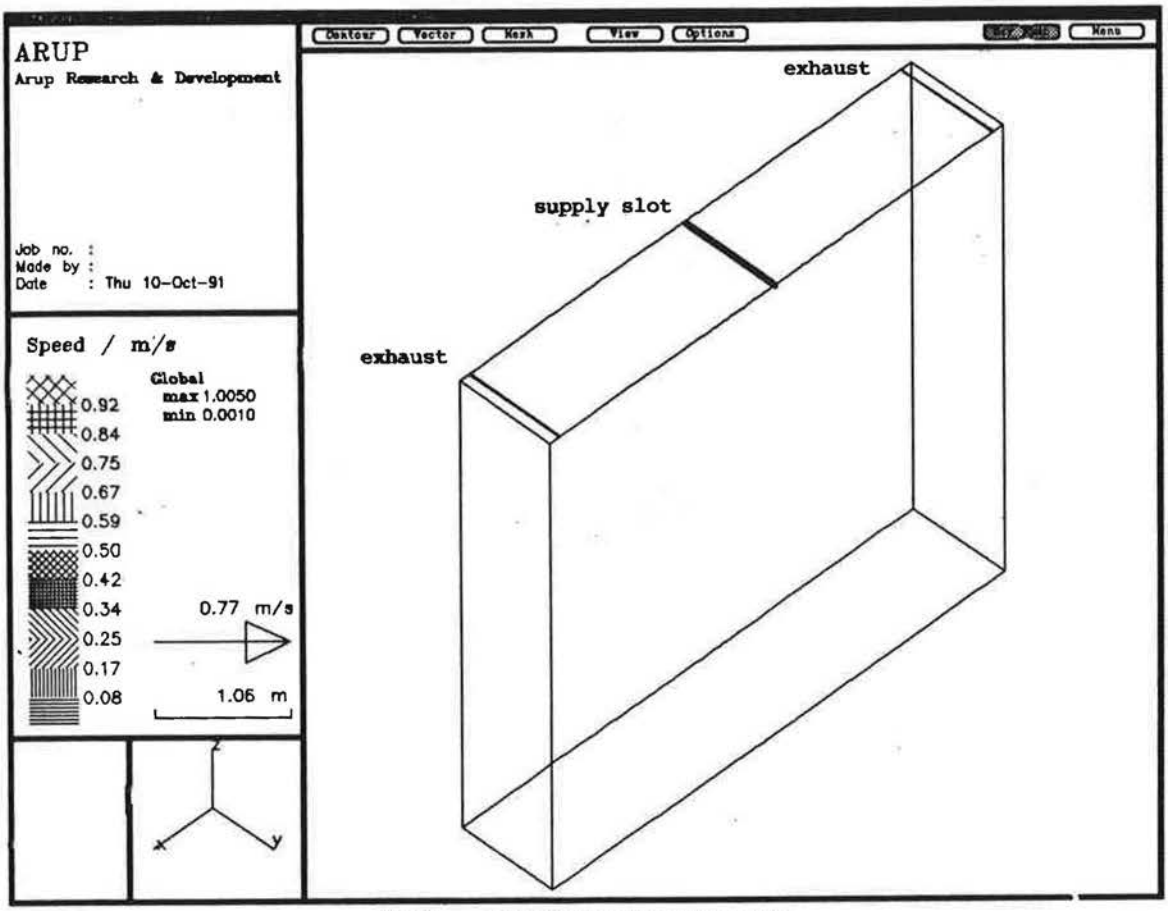

Fig 1 Schematic of room module

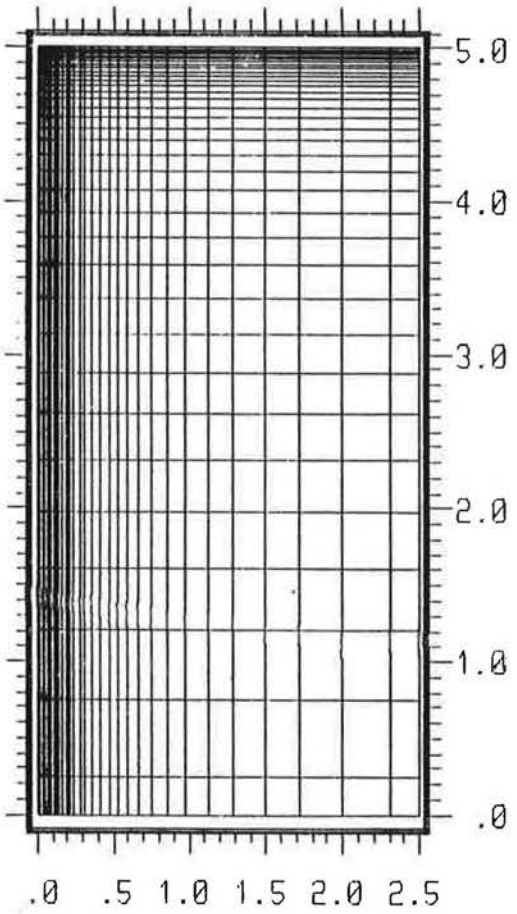

Fig 2 40 x 40 mesh (half room)

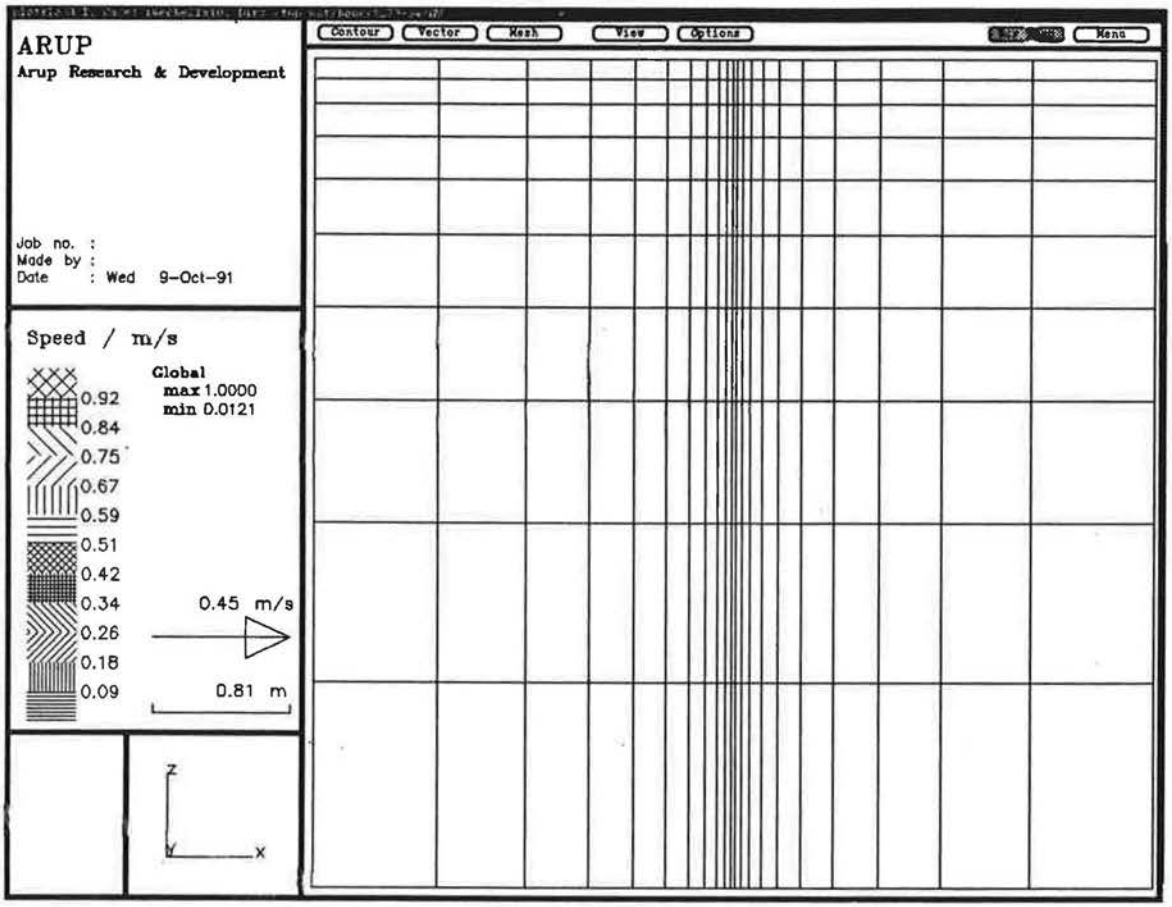

Fig 3 21 x 10 mesh (full room)

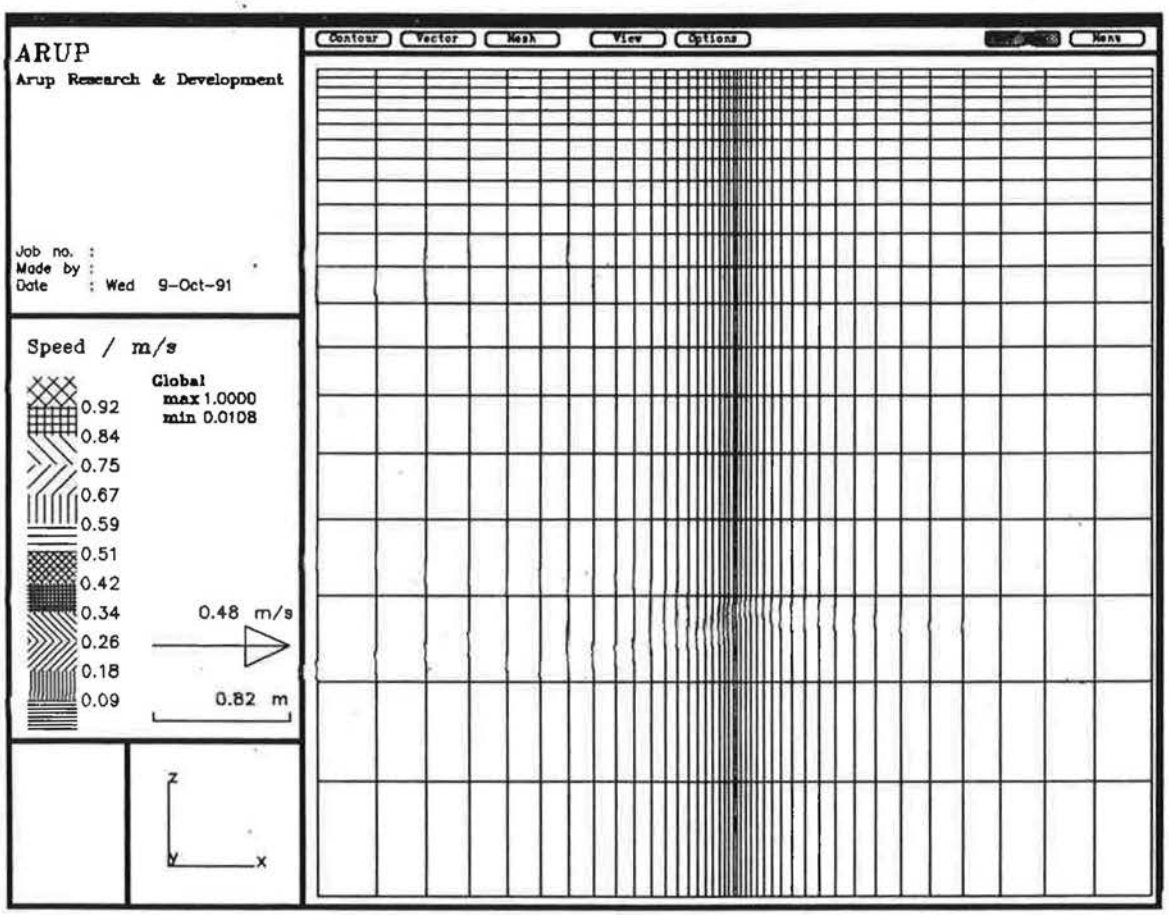

Fig 4 41 x 20 mesh (full room)

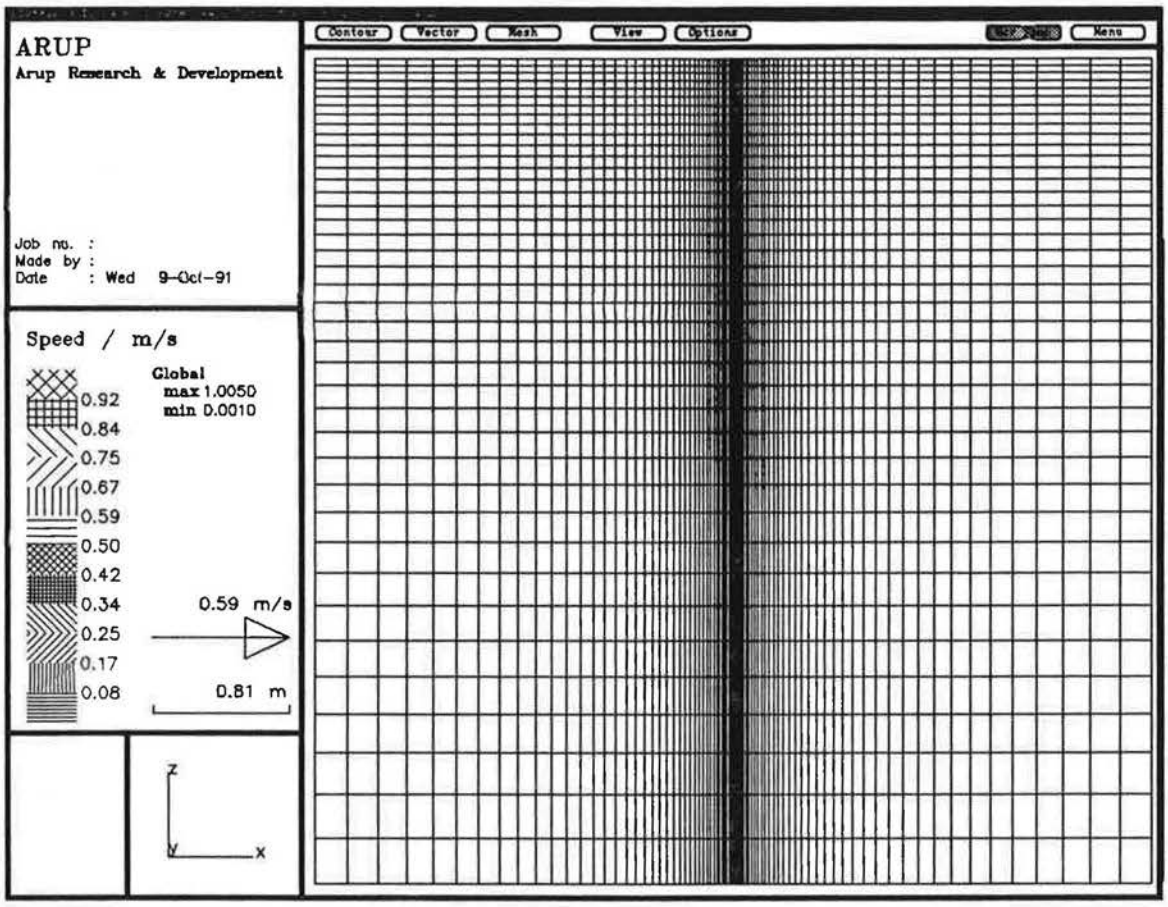

Fig 5 40 x 40 mesh (full room)

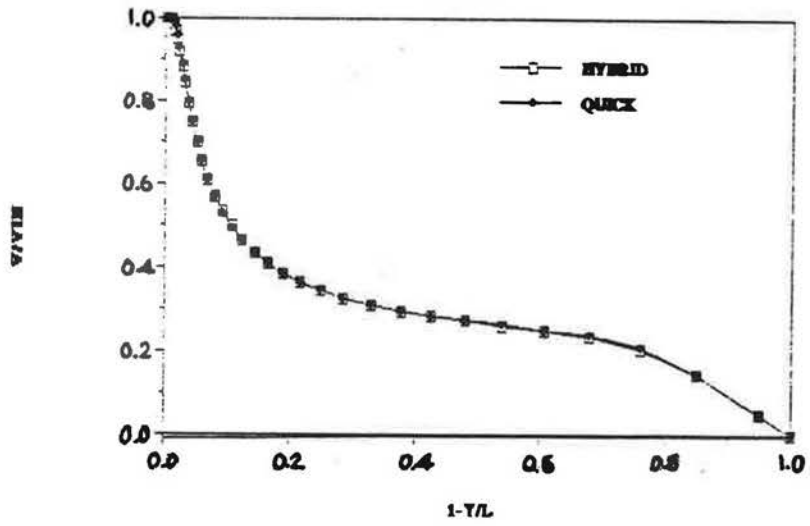

Fig 6 Isothermal velocity decay (hybrid and quick differencing) 40 x 40 mesh

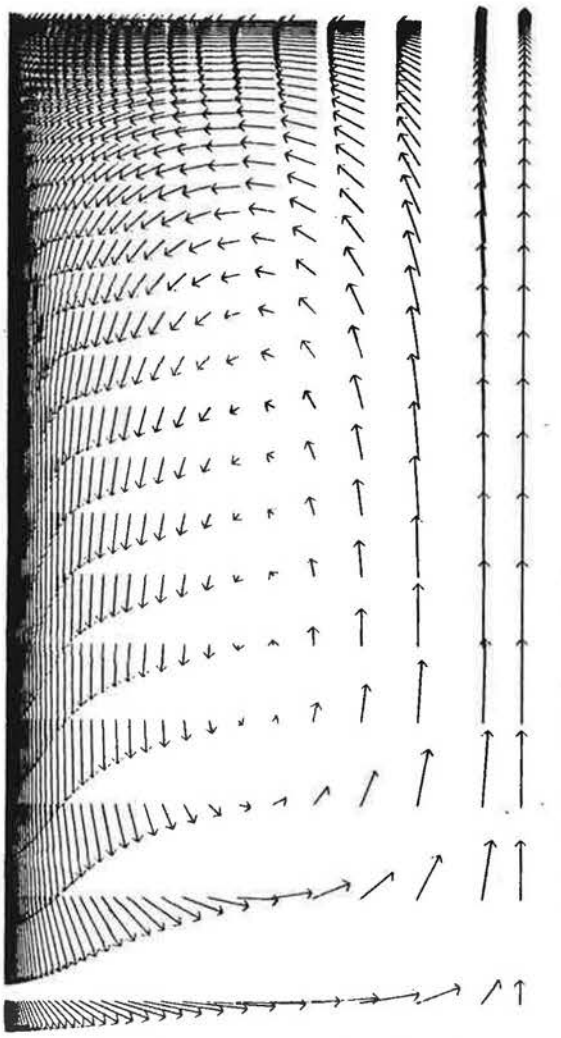

Fig 7 Velocity vectors (isothermal)
40 x 40 mesh

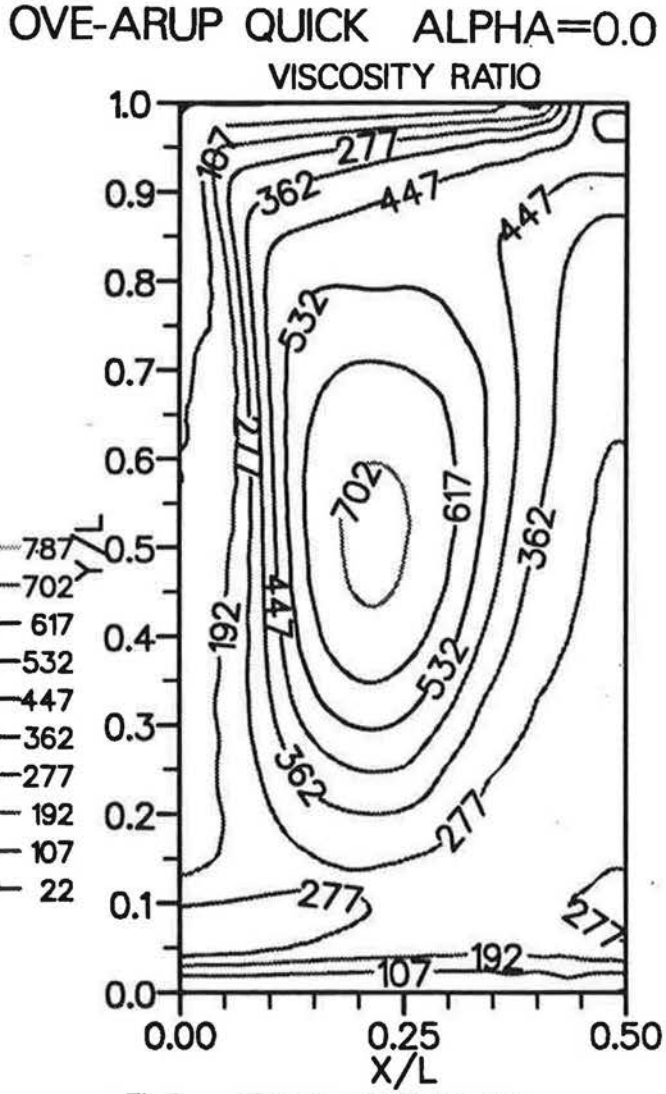

Fig 8 Viscosity ratio (isothermal)
40 x 40 mesh

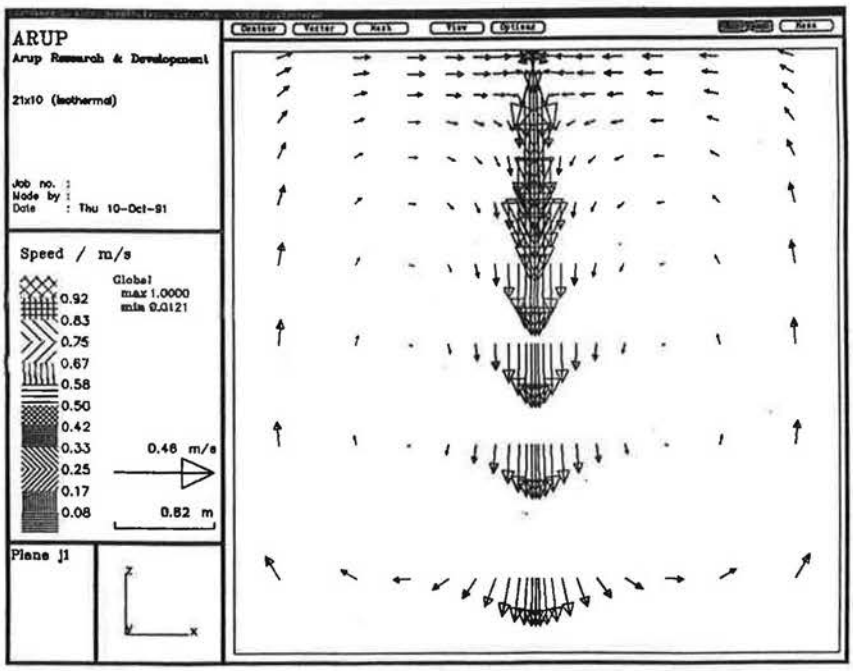

Fig 9 Velocity vectors (isothermal)
21 x 10 mesh

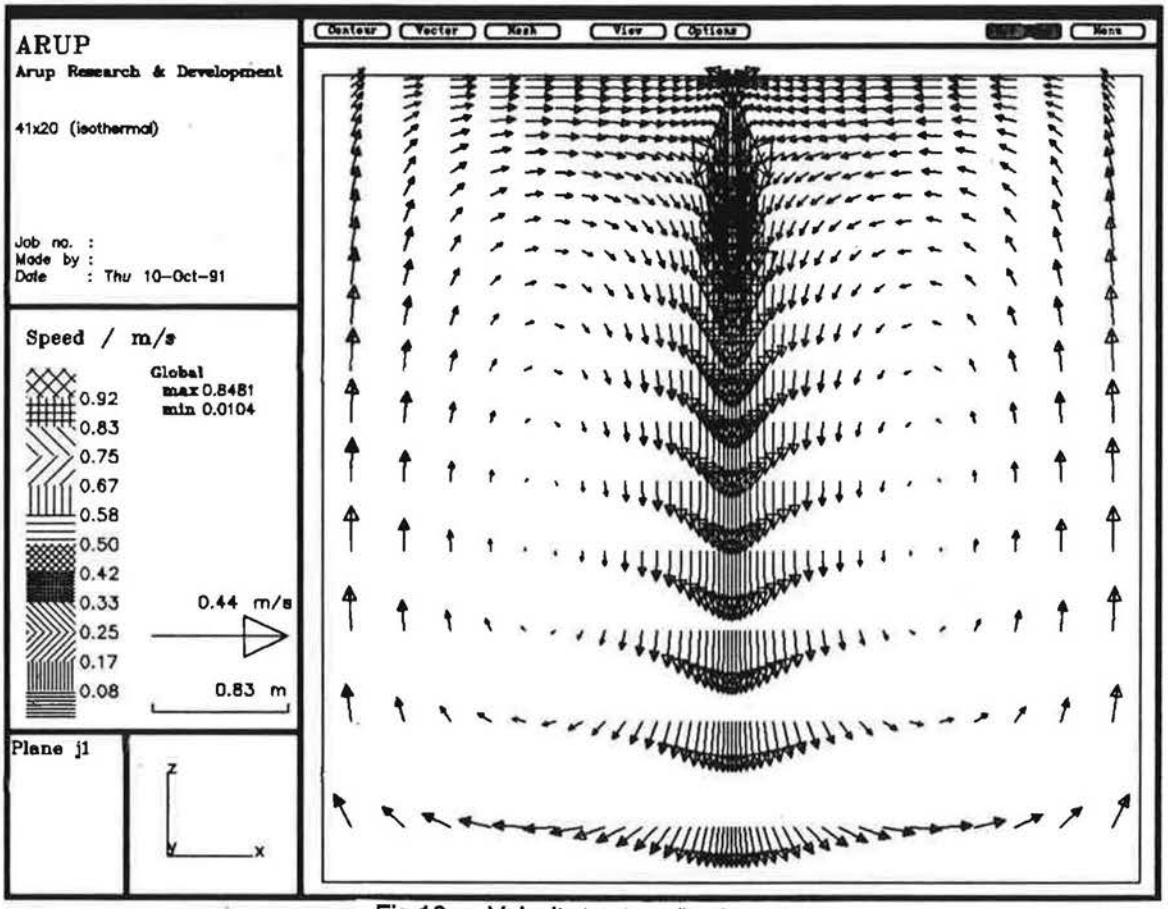

Fig 10 Velocity vectors (isothermal)
41 x 20 mesh

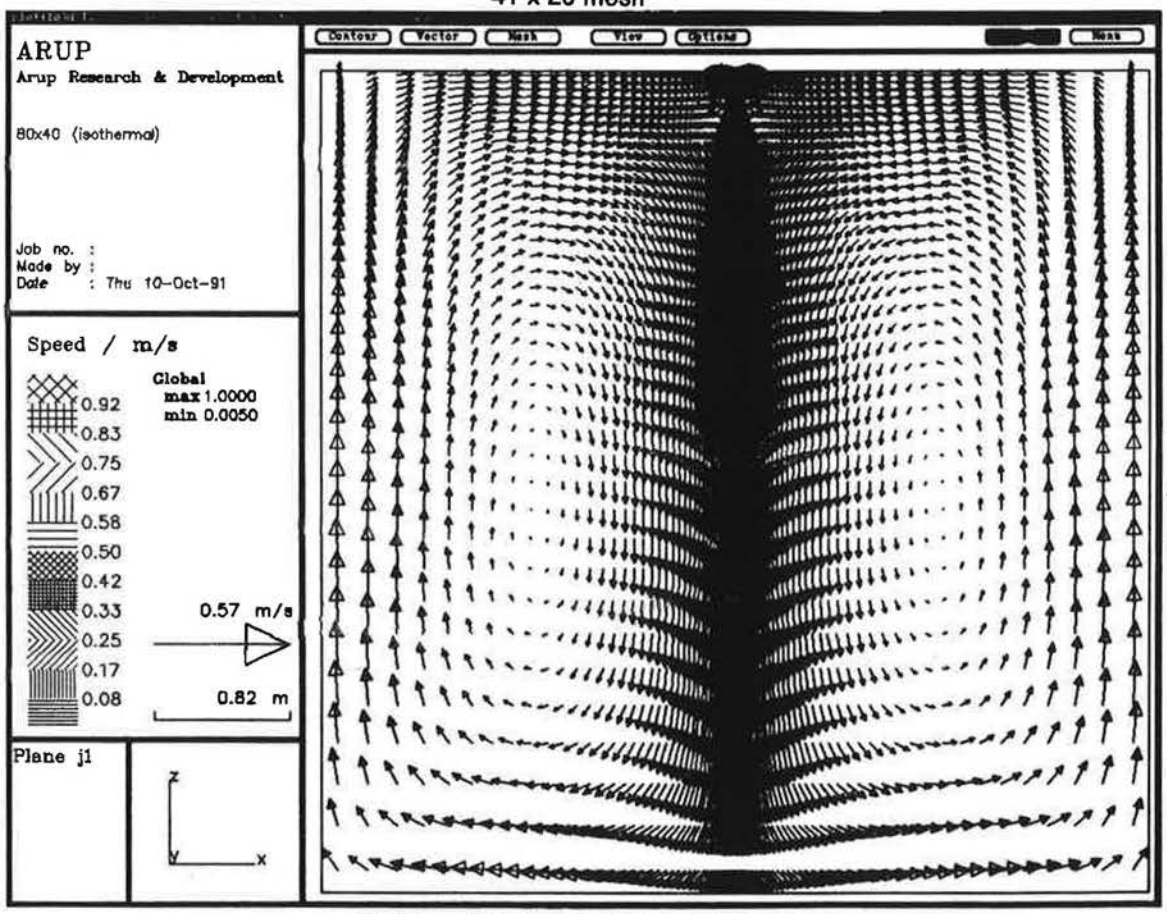

Fig 11 Velocity vectors (isothermal)
80 x 40 mesh

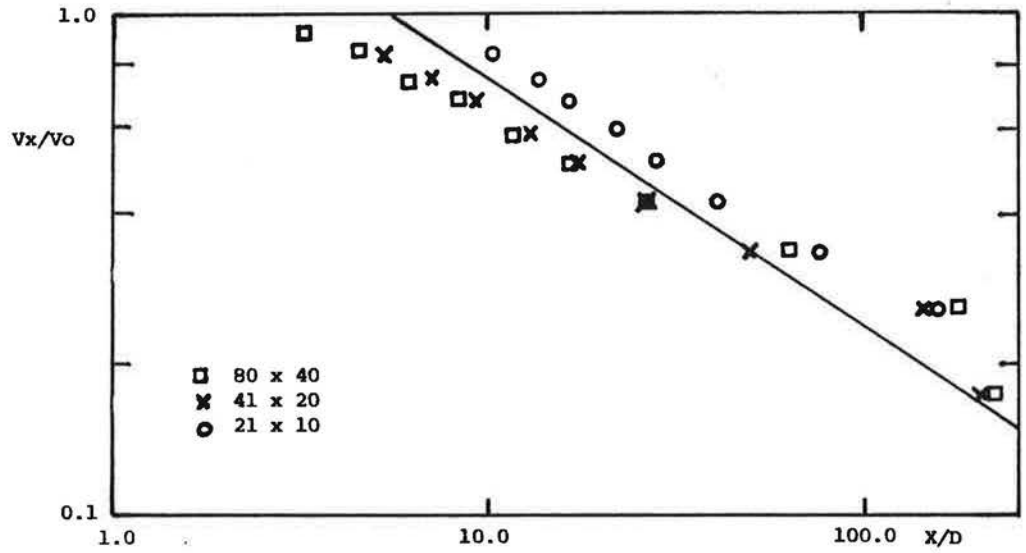

Fig 12 Velocity decay (isothermal)

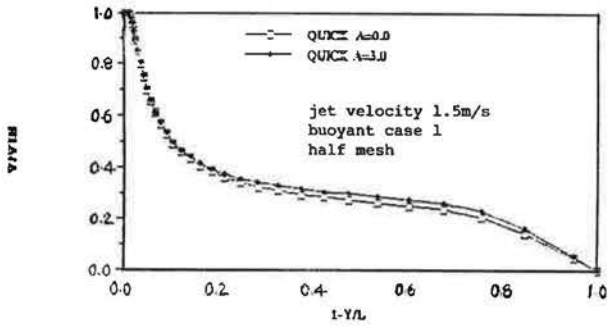

Fig 13 Velocity decay (isothermal and buoyant)

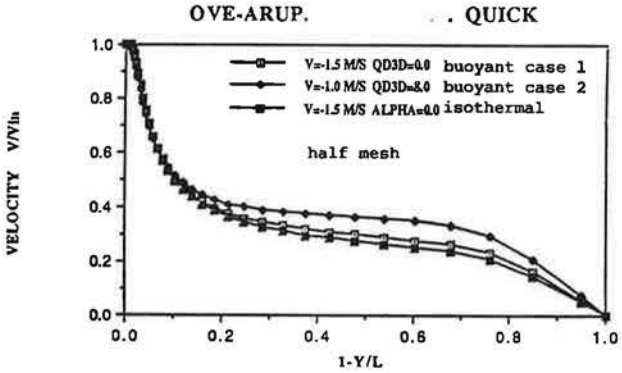

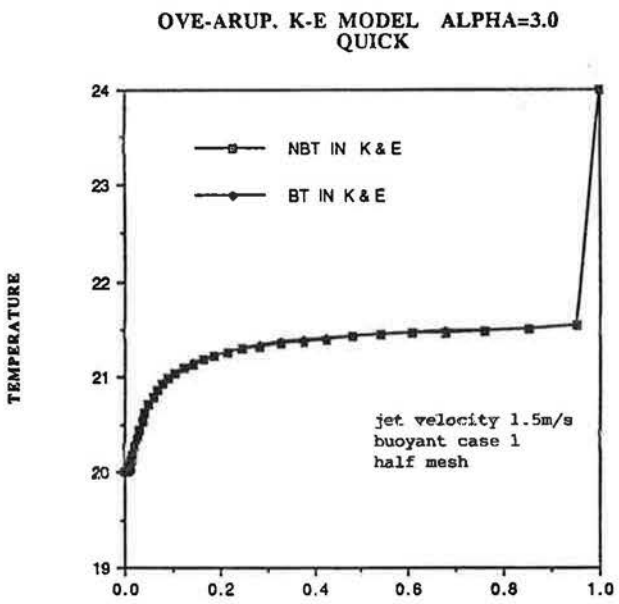

Fig 14 Temperature rise (influence of buoyancy terms in KE model)

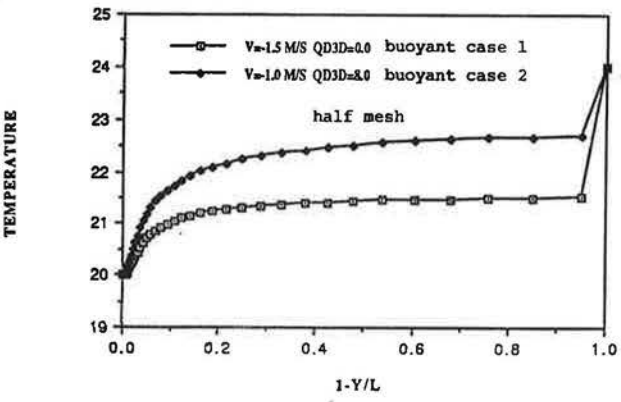

Fig 15 Velocity and temperature decay (influence of buoyancy)

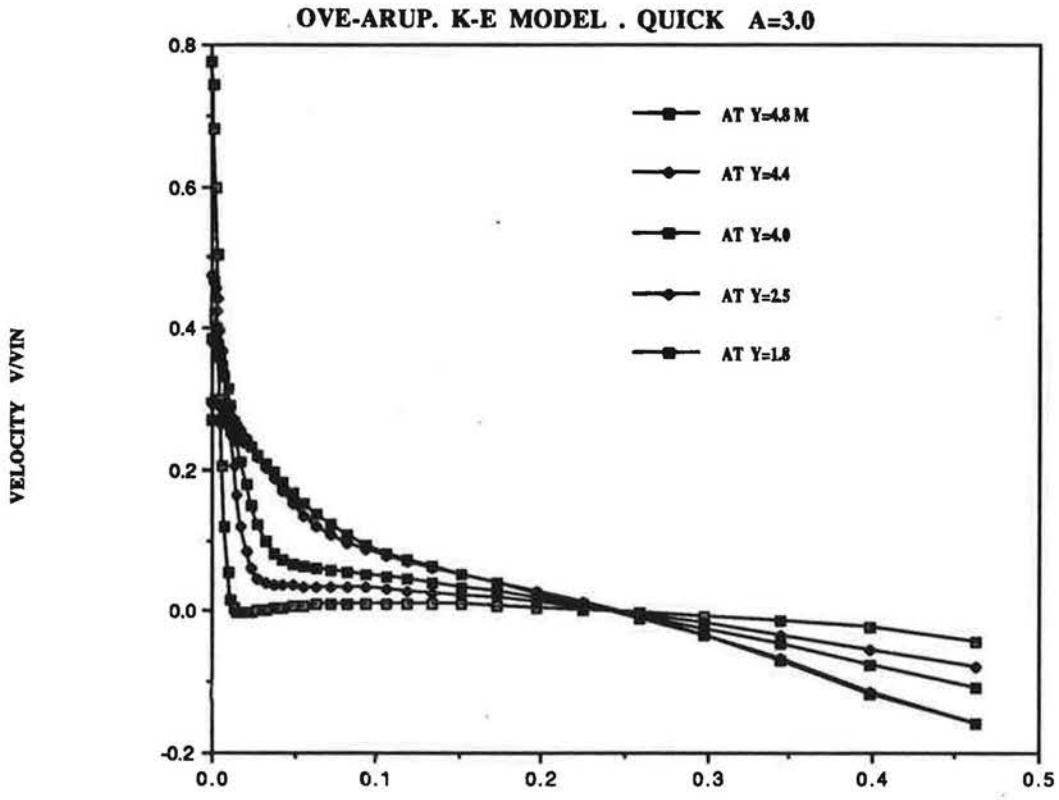

Fig 16 Vertical velocity profiles (buoyancy case 1)

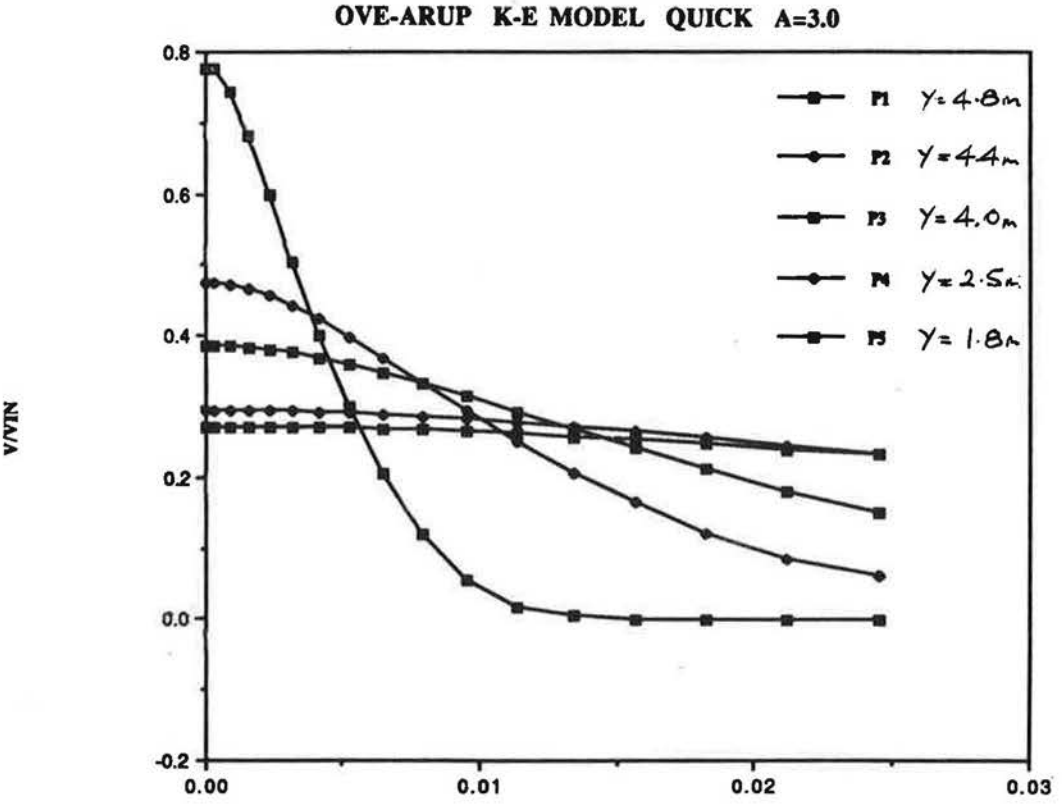

Fig 17 Vertical velocity profiles in jet vicinity (buoyancy case 1)

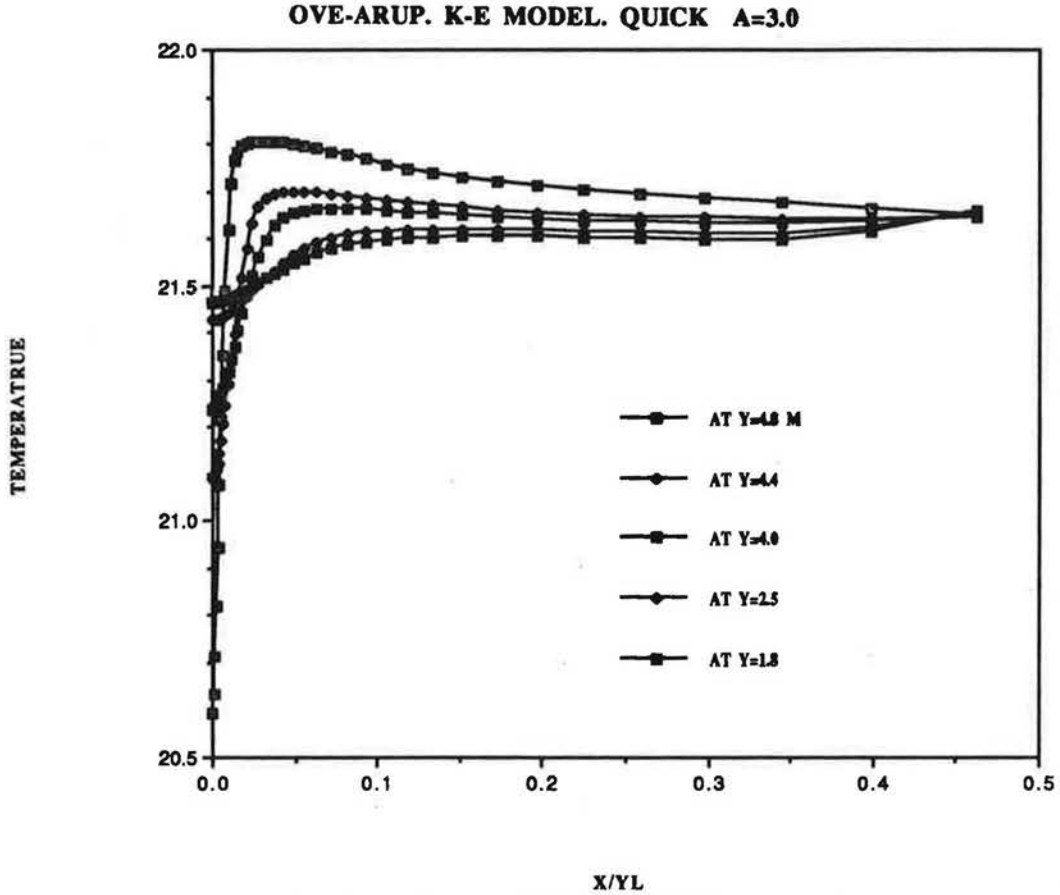

Fig 18 Temperature profiles (buoyancy case 1)

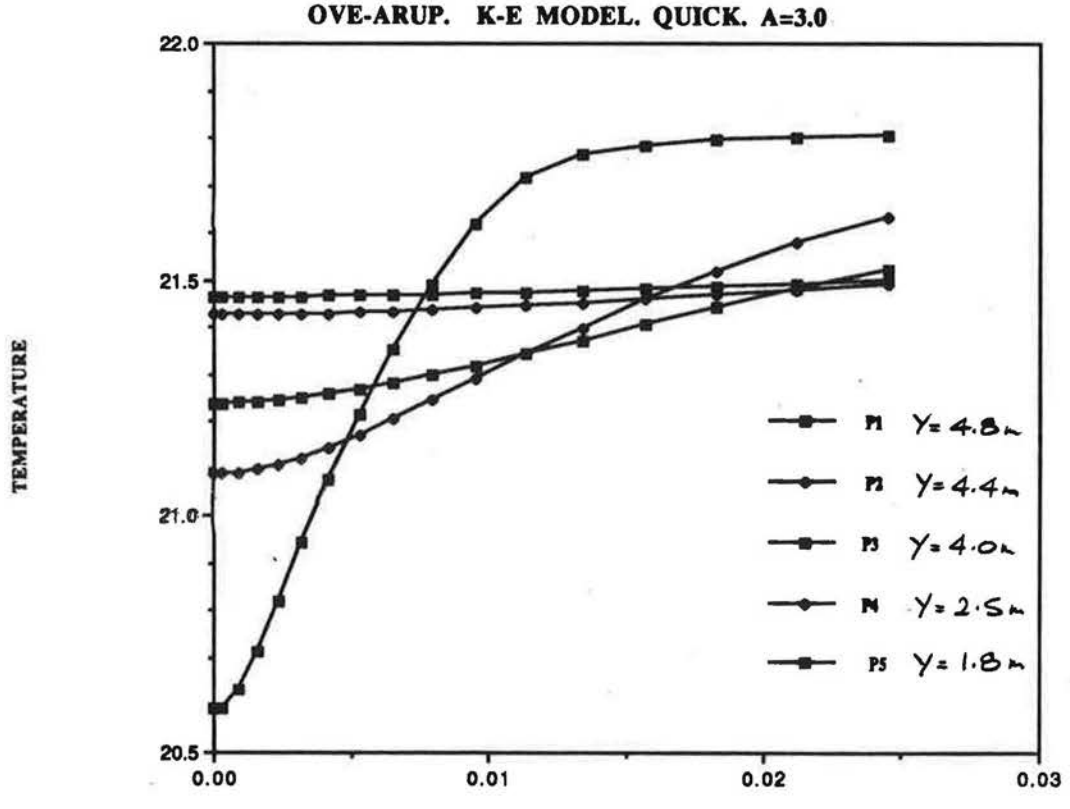

Fig 19 Temperature profiles in jet vicinity (buoyancy case 1)

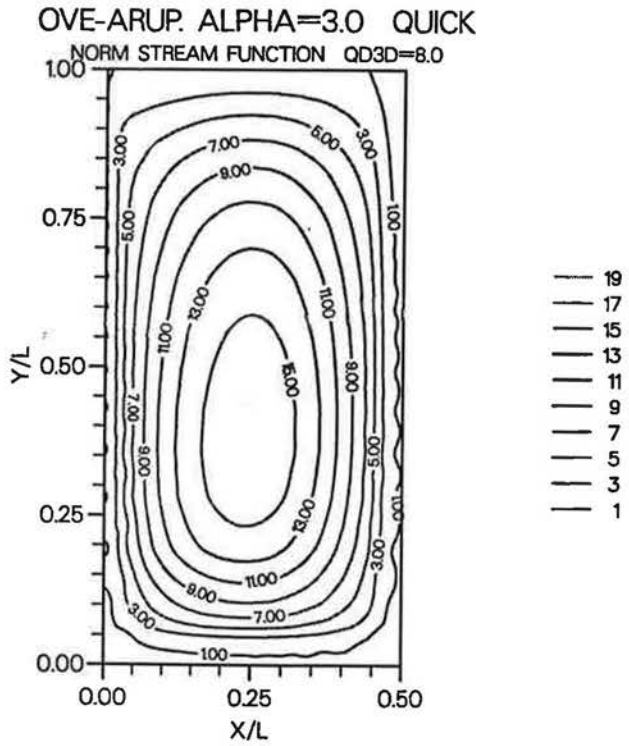

Fig 20 Normalised stream function (buoyancy case 2)

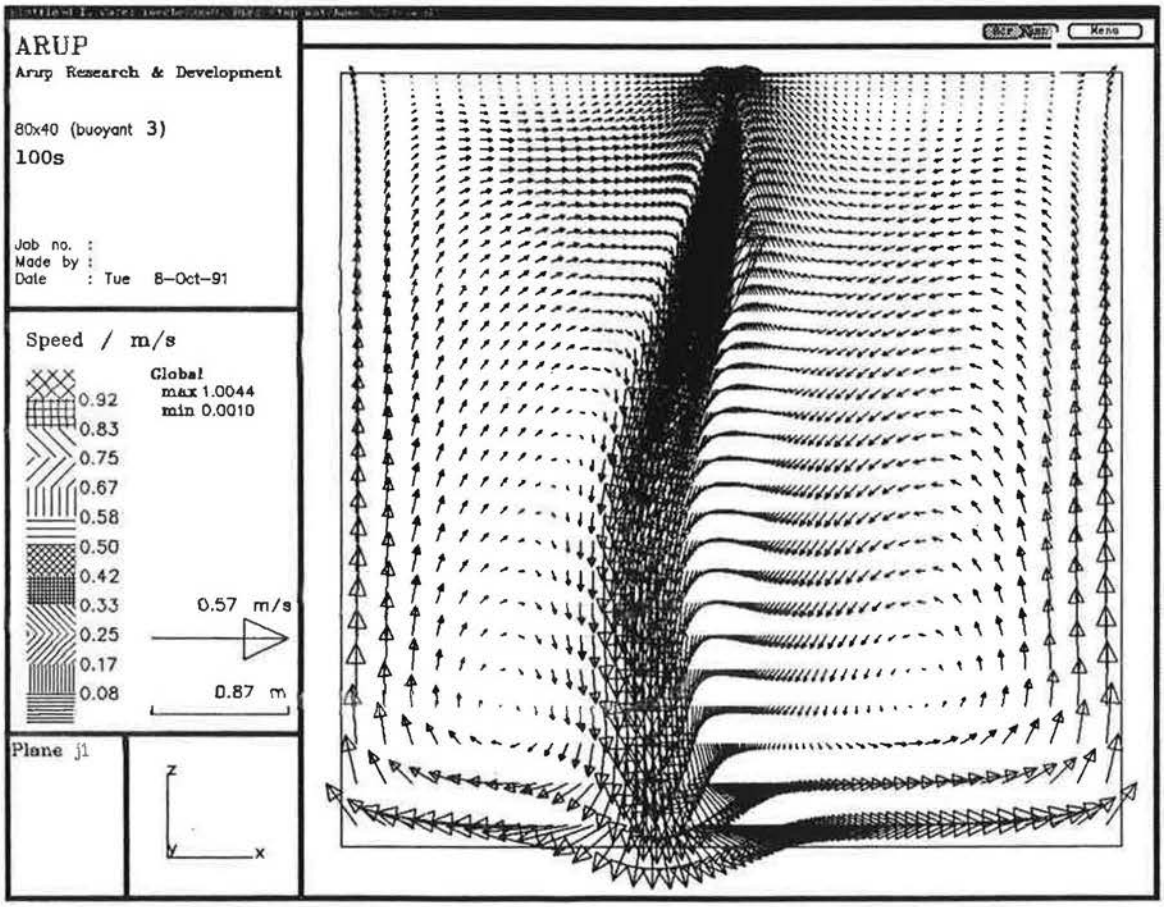

Fig 21 Velocity vectors at t seconds (strong buoyancy 10°C)

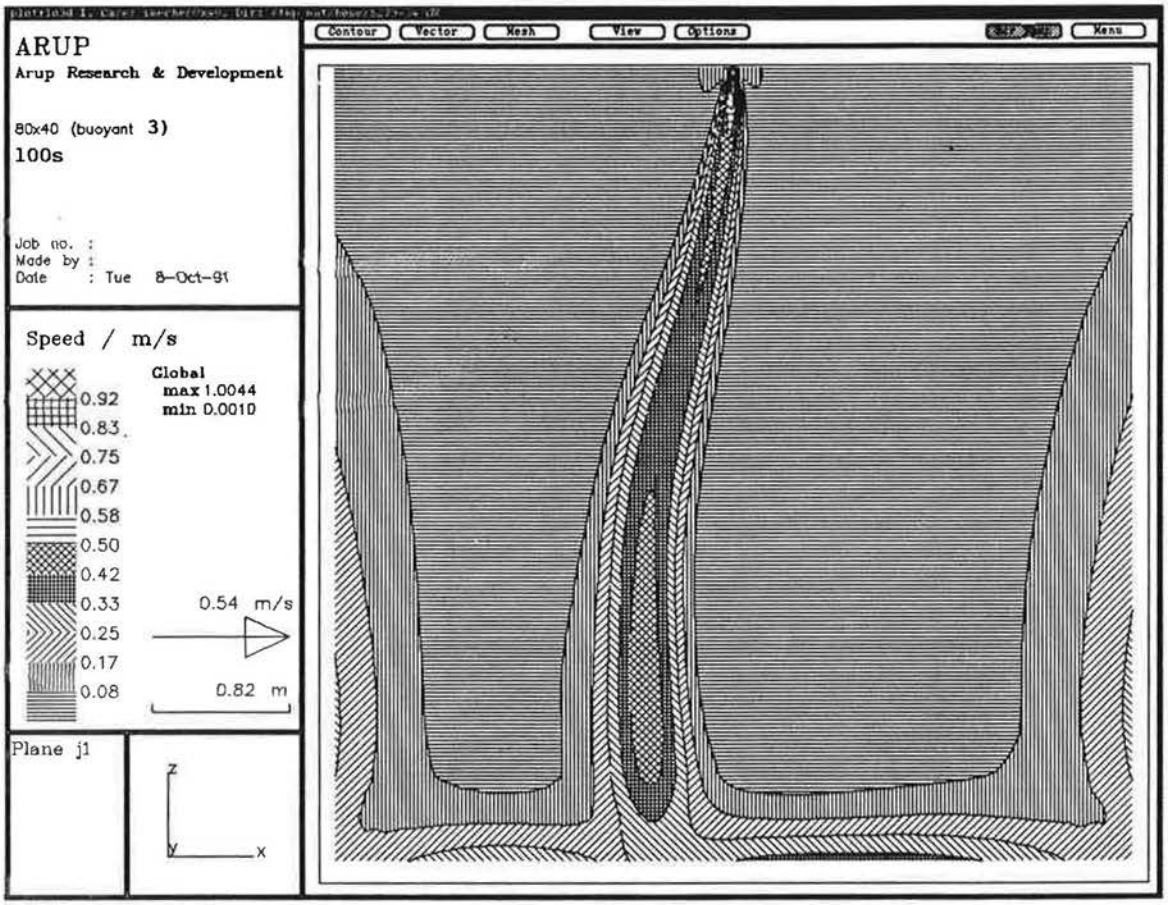

Fig 22 Speed contours at t seconds
(strong buoyancy 10°C)

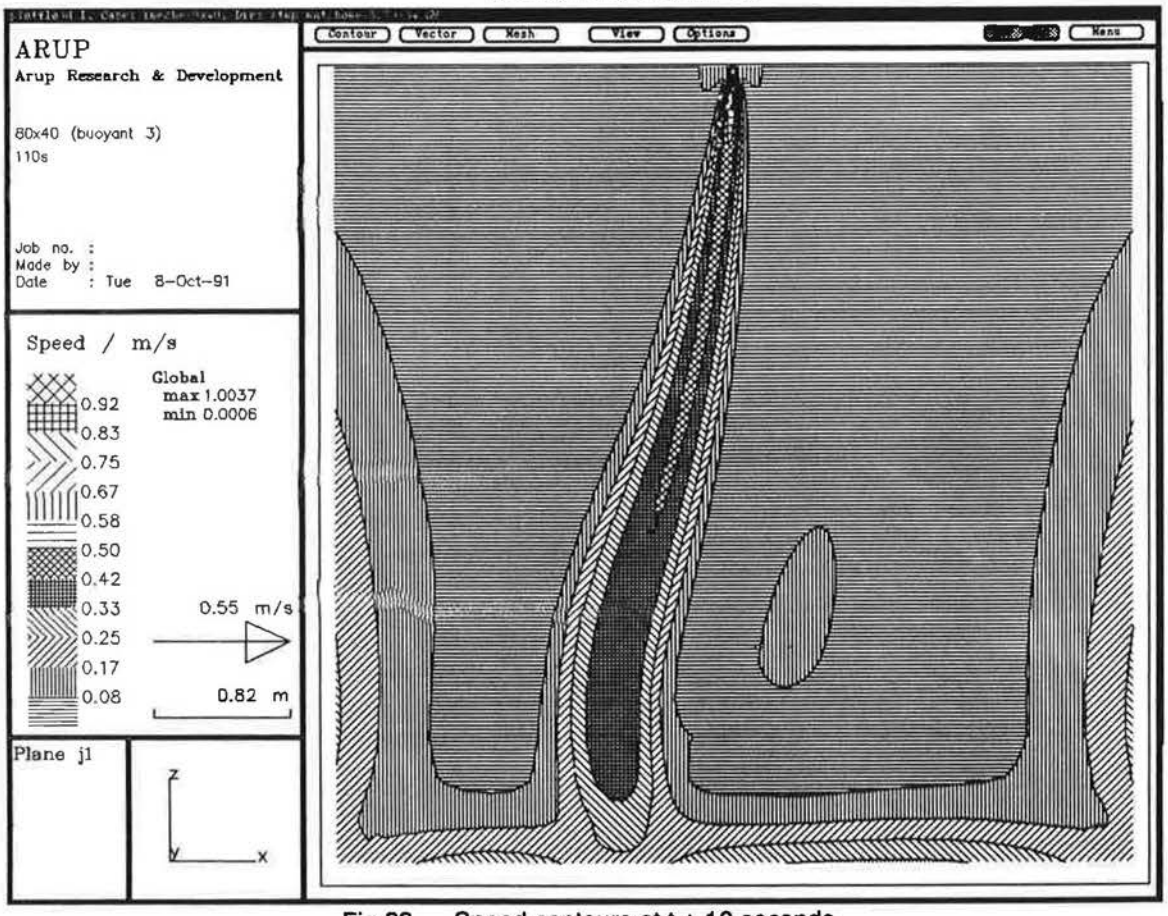

Fig 23 Speed contours at t + 10 seconds
(strong buoyancy 10°C)

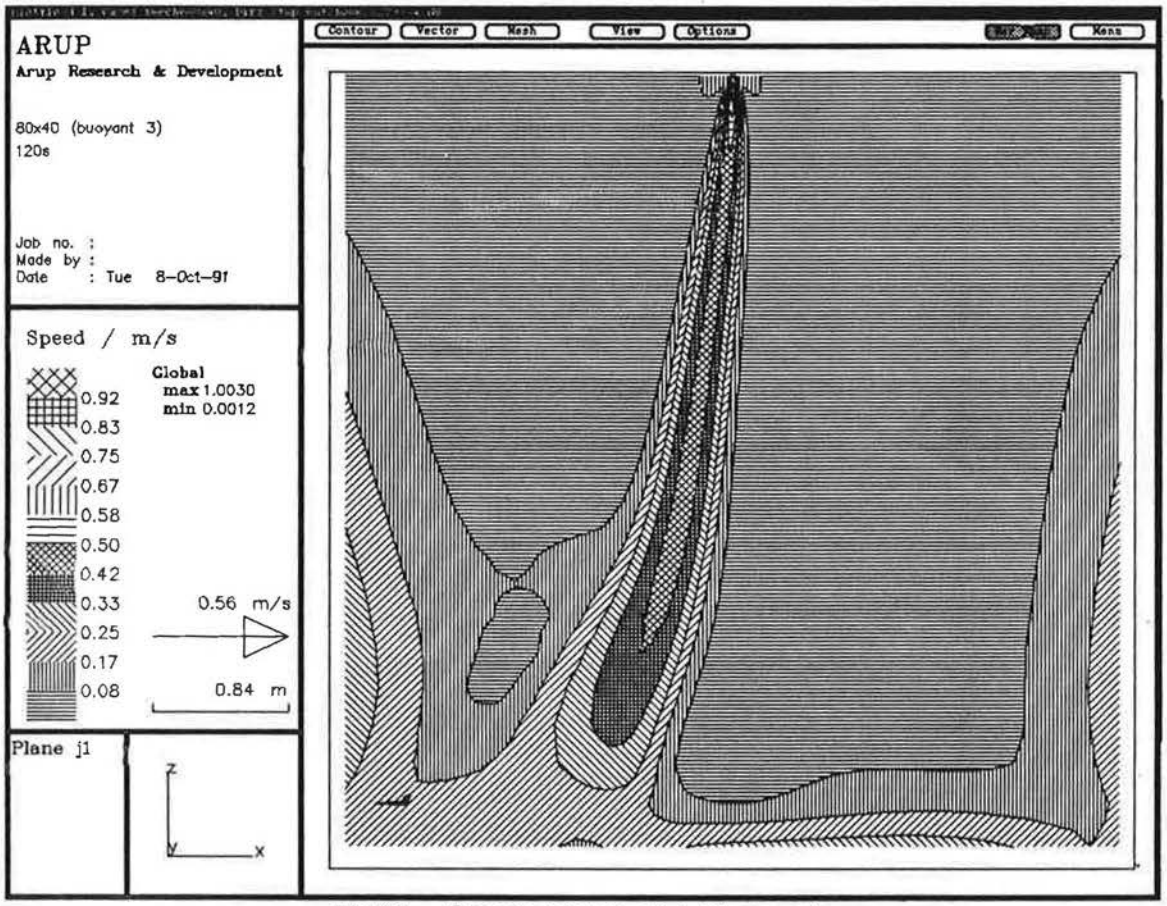

Fig 24 Speed contours at t + 20 seconds
(strong buoyancy 10°C)

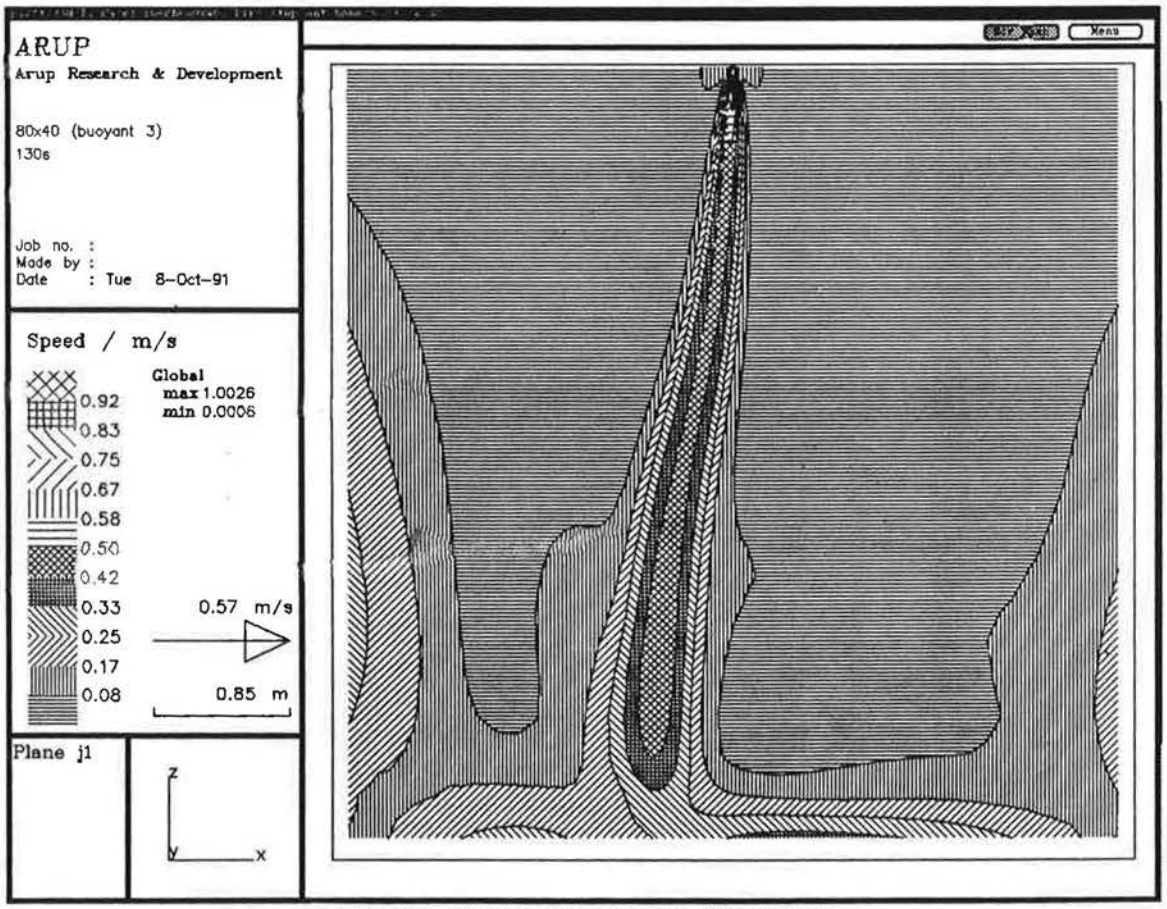

Fig 25 Speed contours at t + 30 seconds
(strong buoyancy 10°C)

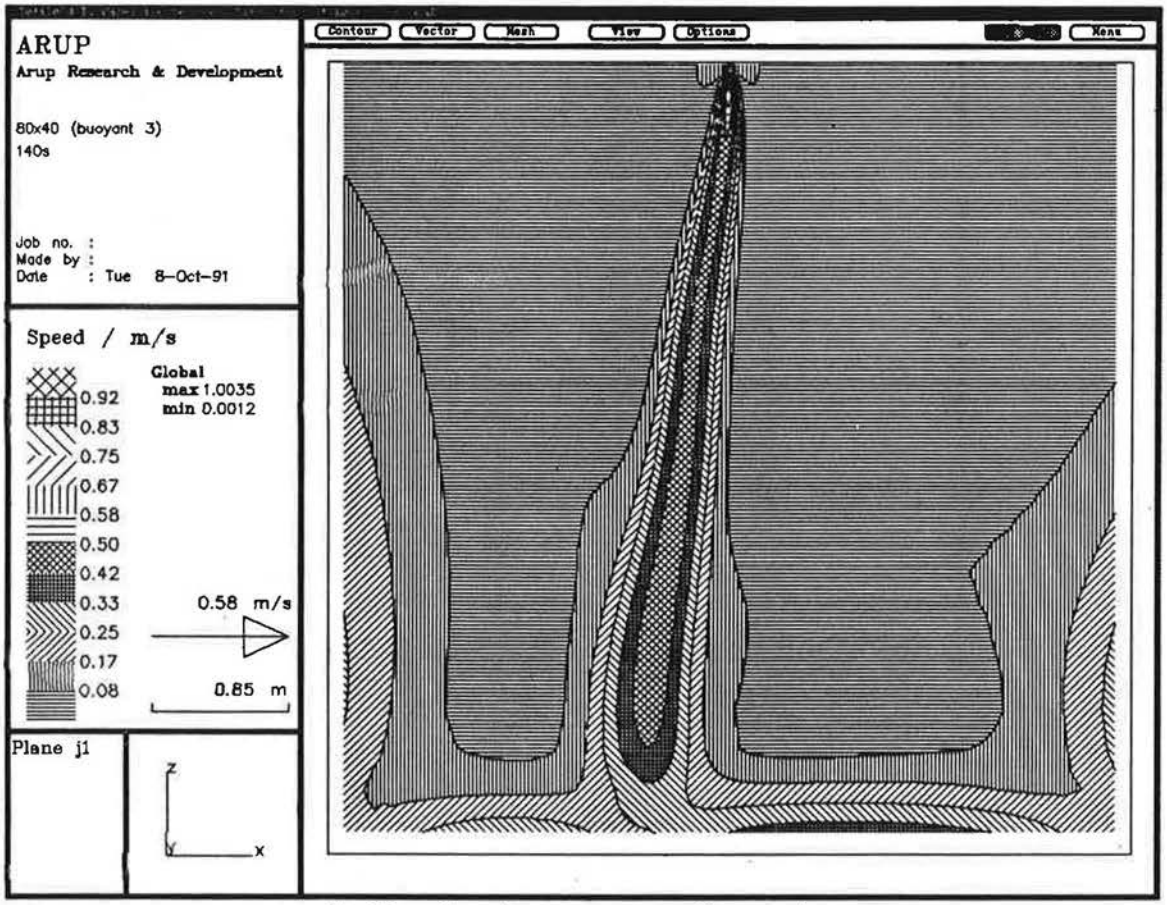

Fig 26 Speed contours at t + 40 seconds (strong buoyancy 10°C)

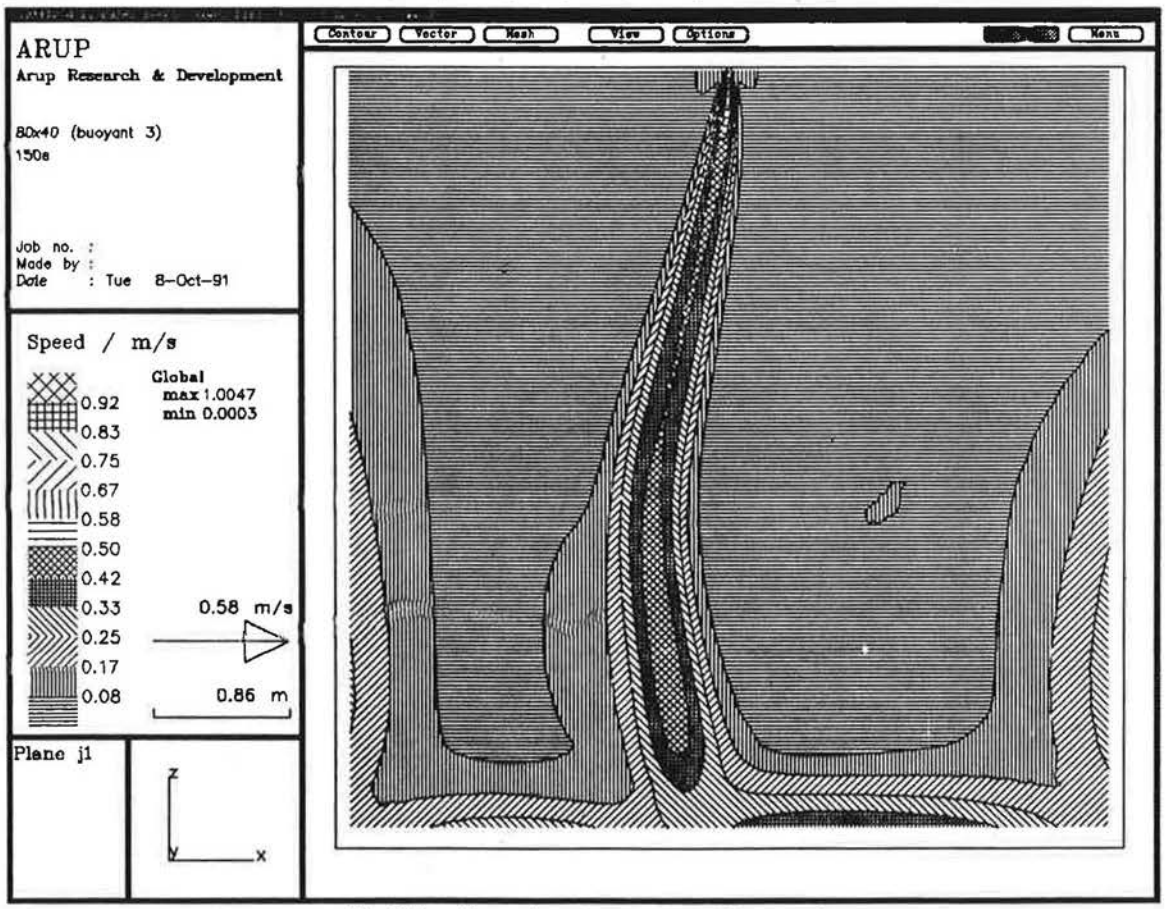

Fig 27 Speed contours at t + 50 seconds (strong buoyancy 10°C)

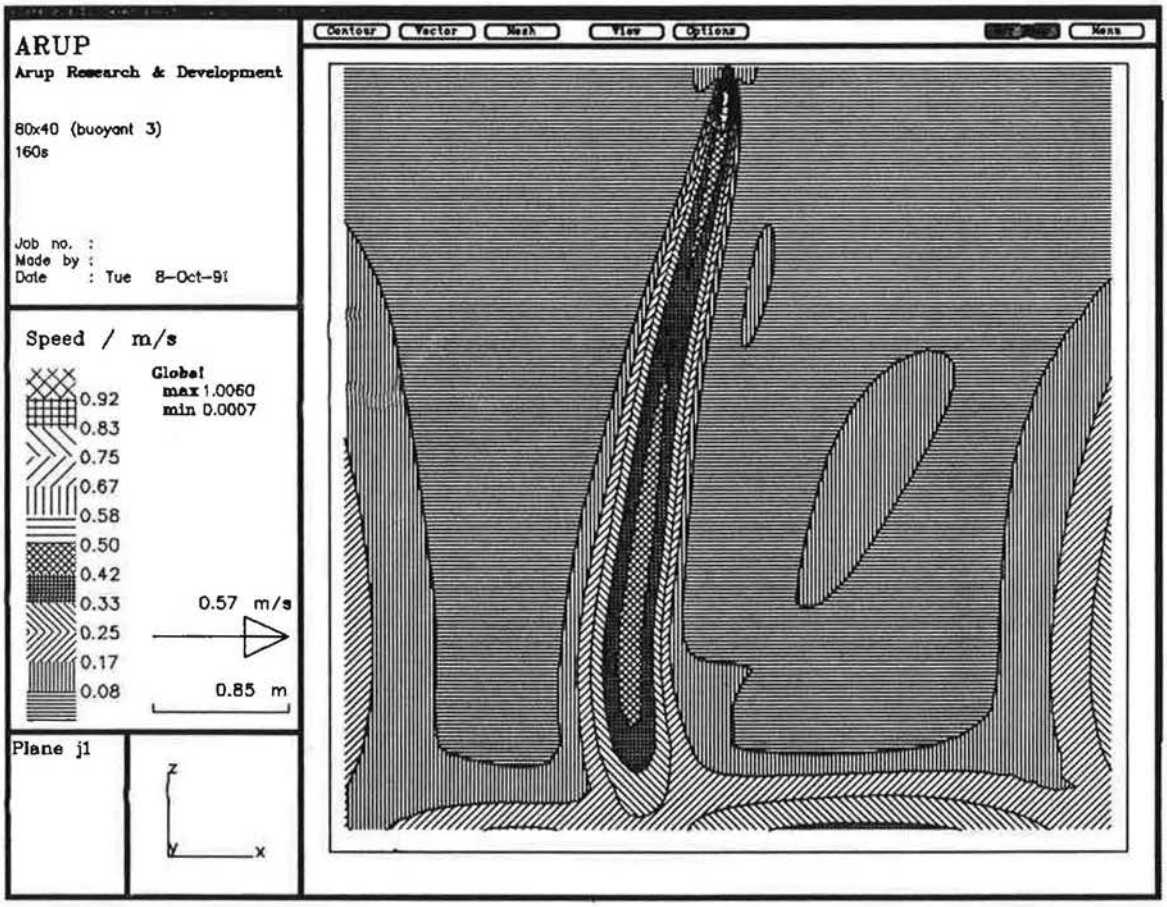

Fig 28 Speed contours at t + 60 seconds (strong buoyancy 10°C)

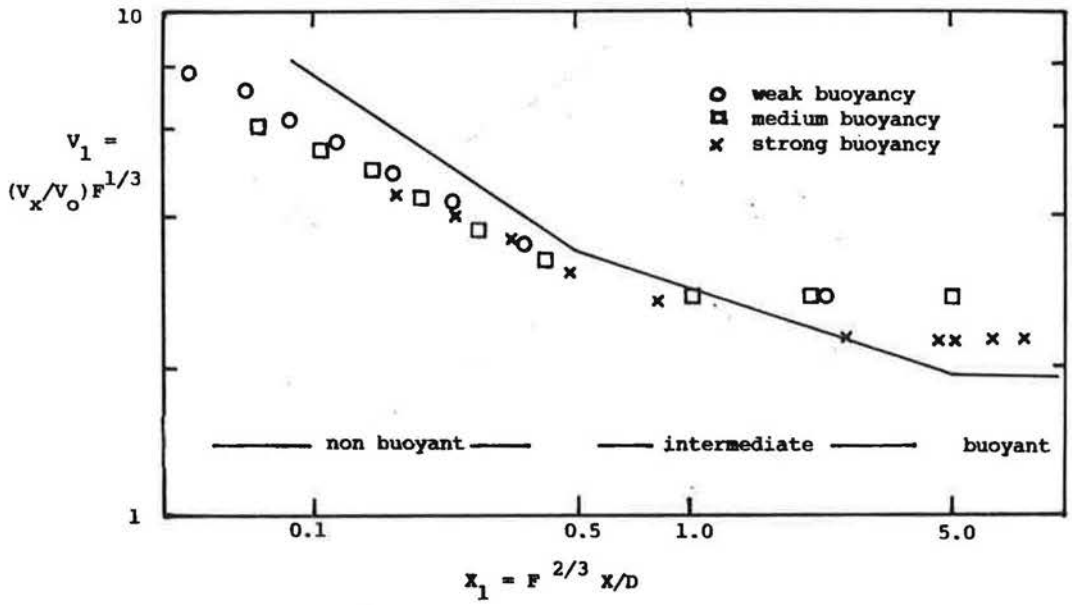

Fig 29 Velocity decay (comparison with Chen and Rodi (12))

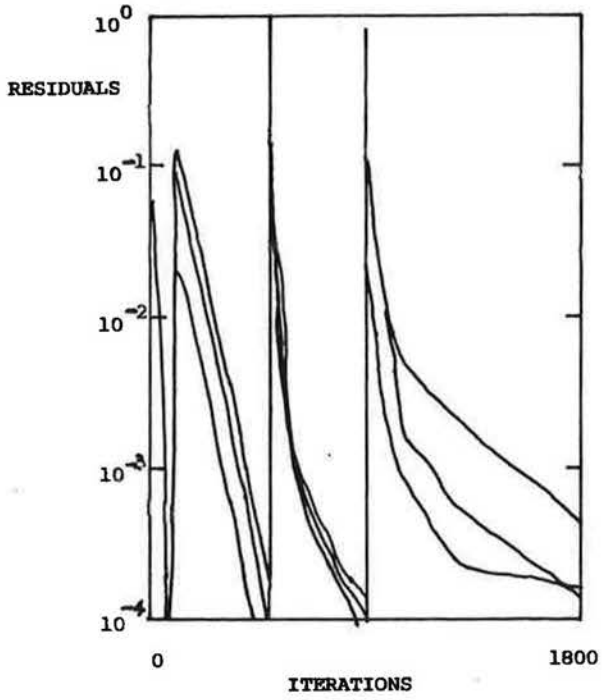

Fig 30 Residual errors (3 meshes) weak buoyancy

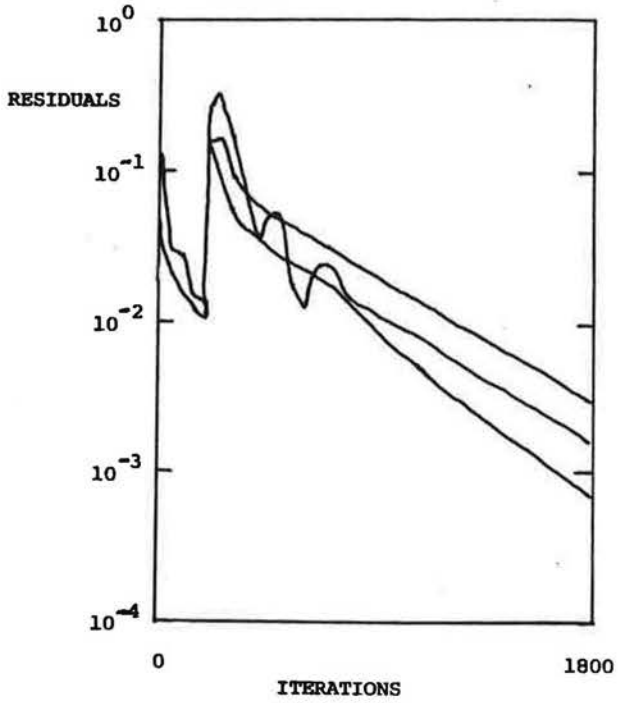

Fig 31 Residual errors (single mesh) weak buoyancy

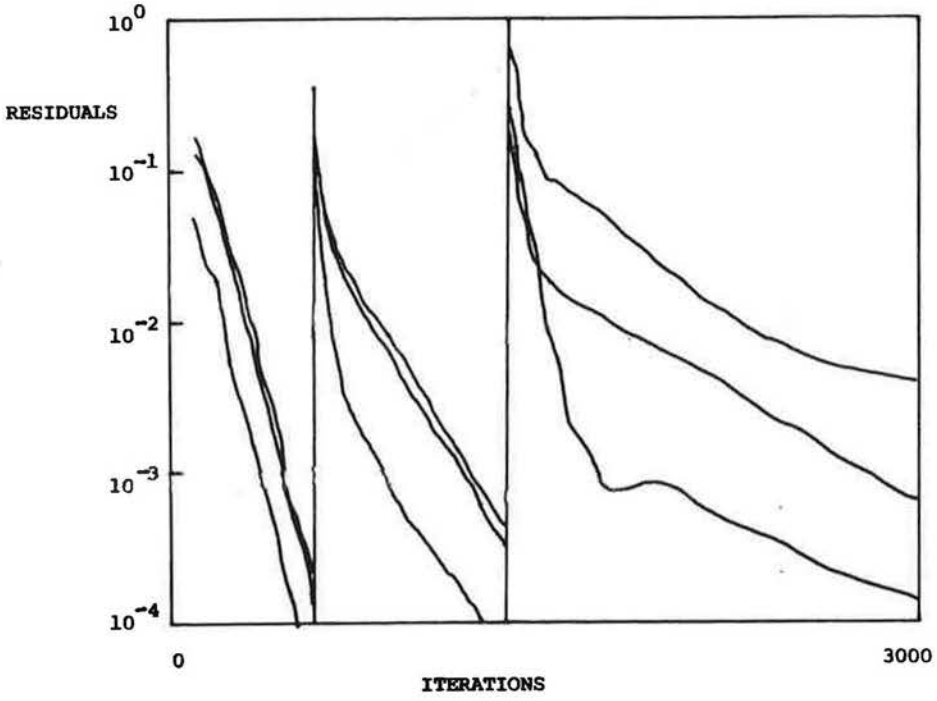

Fig 32 Residual errors (3 meshes) medium buoyancy